Current Biology 20, 103–115, January 26, 2010 ©2010 Elsevier Ltd All rights reserved DOI 10.1016/j.cub.2009.12.030

Article

A Postsynaptic Signaling Pathway that May Account for the Cognitive Defect Due to IL1RAPL1 Mutation

Alice Pavlowsky,[1,2,11] Antonella Gianfelice,[3,11] Marta Pallotto,[4,11] Alice Zanchi,[3] Hugo Vara,[4] Malik Khelfaoui,[1,2,5] Pamela Valnegri,[3,6] Xavier Rezai,[7] Silvia Bassani,[3,6] Dario Brambilla,[8] Jiri Kumpost,[9] Jaroslav Blahos,[9] Michel J. Roux,[7] Yann Humeau,[5] Jamel Chelly,[1,2] Maria Passafaro,[3,6] Maurizio Giustetto,[4] Pierre Billuart,[1,2,*] and Carlo Sala[3,10,*]

[1]Department of Genetics and Development, Institut Cochin, Université Paris Descartes, Centre National de la Recherche Scientifique (CNRS) Unité Mixte de Recherche (UMR) 8104, 75014 Paris, France

[2]Inserm U567, 75014 Paris, France

[3]CNR Neuroscience Institute and Department of Pharmacology, University of Milan, 20129 Milan, Italy

[4]National Institute of Neuroscience-Italy and Department of Anatomy, Pharmacology and Forensic Medicine, University of Turin, 10126 Turin, Italy

[5]Institut des Neurosciences Cellulaires et Intégratives, UPR3212, CNRS, 67084 Strasbourg, France

[6]Dulbecco Telethon Institute, 20129 Milano, Italy

[7]Institut de Génétique et de Biologie Moléculaire et Cellulaire-Institut de la Souris (IGBMC-ICS), 1 rue Laurent Fries BP10142, 67404 Illkirch cedex, France

[8]Department of Human Physiology, University of Milan, 20133 Milan, Italy

[9]Department of Molecular Pharmacology, Institute of Molecular Genetics AS CR, 142 20 Prague 4, Czech Republic

[10]Neuromuscular Diseases and Neuroimmunology, Neurological Institute Foundation "Carlo Besta," 20133 Milan, Italy

Summary

Background: *I*nter*l*eukin-*1 r*eceptor *a*ccessory *p*rotein-*l*ike *1* (*IL1RAPL1*) gene mutations are associated with cognitive impairment ranging from nonsyndromic X-linked mental retardation to autism. IL1RAPL1 belongs to a novel family of Toll/IL-1 receptors, whose expression in the brain is upregulated by neuronal activity. Currently, very little is known about the function of this protein. We previously showed that IL1RAPL1 interacts with the neuronal calcium sensor NCS-1 and that it regulates voltage-gated calcium channel activity in PC12 cells.
Results: Here we show that IL1RAPL1 is present in dendritic spine where it interacts with PSD-95, a major component of excitatory postsynaptic compartment. Using gain- and loss-of-function experiments in neurons, we demonstrated that IL1RAPL1 regulates the synaptic localization of PSD-95 by controlling c-*Jun* terminal *k*inase (JNK) activity and PSD-95 phosphorylation. Mice carrying a null mutation of the mouse *Il1rapl1* gene show a reduction of both dendritic spine density and excitatory synapses in the CA1 region of the hippocampus. These structural abnormalities are associated with specific deficits in hippocampal long-term synaptic plasticity.
Conclusion: The interaction of IL1RAPL1 with PSD-95 discloses a novel pathophysiological mechanism of cognitive impairment associated with alterations of the JNK pathway leading to a mislocalization of PSD-95 and abnormal synaptic organization and function.

*Correspondence: pierre.billuart@inserm.fr (P.B.), c.sala@in.cnr.it (C.S.)
[11]These authors contributed equally to this work

Introduction

Mental retardation (MR) is defined by an overall "intelligence quotient" lower than 70, with an onset before 18 years of age. It affects about 2%–3% of the human population. The underlying causes of MR are extremely heterogeneous; they include environmental and genetic factors, many of which are X-linked conditions [1]. The first mutation in *IL1RAPL1* gene, described by Carrié et al. [2], was associated with nonsyndromic MR. Similar to some other genes involved in cognitive impairment [3], *IL1RAPL1* mutations are associated with a spectrum of cognitive impairment ranging from MR to autism [4]. IL1RAPL1 belongs to a novel family of Toll/IL-1 receptors and shares 52% homology with the *IL-1 r*eceptor *a*ccessory *p*rotein (IL-1RacP). As with the other members of IL-1 receptor family, it is characterized by three extracellular Ig-like domains, a transmembrane domain, and an intracellular Toll/IL-1R homology domain (TIR domain), plus, unlike the others, 150 additional amino acids (aa) at the C-terminal end. The homology with IL-1RacP is evenly distributed throughout the protein with the exception of the last 150 aa, which are present only in IL1RAPL1 and its paralog, IL1RAPL2. We have previously shown that IL1RAPL1 interacts with NCS-1 through this specific region [5] and that this interaction mediates the regulatory effect of IL1RAPL1 overexpression on N-type voltage-gated calcium channel (VGCC) activity in PC12 cells [6].

In this study, we found a novel partner of IL1RAPL1, PSD-95, a major scaffold protein of excitatory synapses that is known to promote their maturation and strengthening [7, 8]. In order to understand the physiological role of this interaction, we studied dendritic spine morphology and PSD-95 distribution in both gain- and loss-of-IL1RAPL1-function experiments. We found that IL1RAPL1 regulates PSD-95 localization to synapses. It has been shown that overexpression of IL1RAPL1 in nonneuronal cells activates the c-Jun terminal kinase (JNK) pathway but not the other pathways classically involved in IL-1 signaling [9, 10]. In neurons, the balance between JNK and PP1 and PP2A activities modulates the phosphorylation level of PSD-95 on Ser-295 and regulates its synaptic localization [11]. Therefore, we tested whether the IL1RAPL1 deficit or overexpression was associated with an imbalance between JNK and PP1 and PP2A phosphatase activity. Finally, to address the in vivo consequences of IL1RAPL1 loss of function, we analyzed the structural organization and the physiological properties of the Schaffer collateral (SC)-CA1 pathway in the hippocampus of IL1RAPL1 knockout (KO) mice [12].

Results

Identification of IL1RAPL1 Interaction with MAGUK Proteins by Yeast Two-Hybrid Screening

In order to identify proteins that interact with IL1RAPL1, we did a yeast two-hybrid screen of a human fetal brain cDNA library

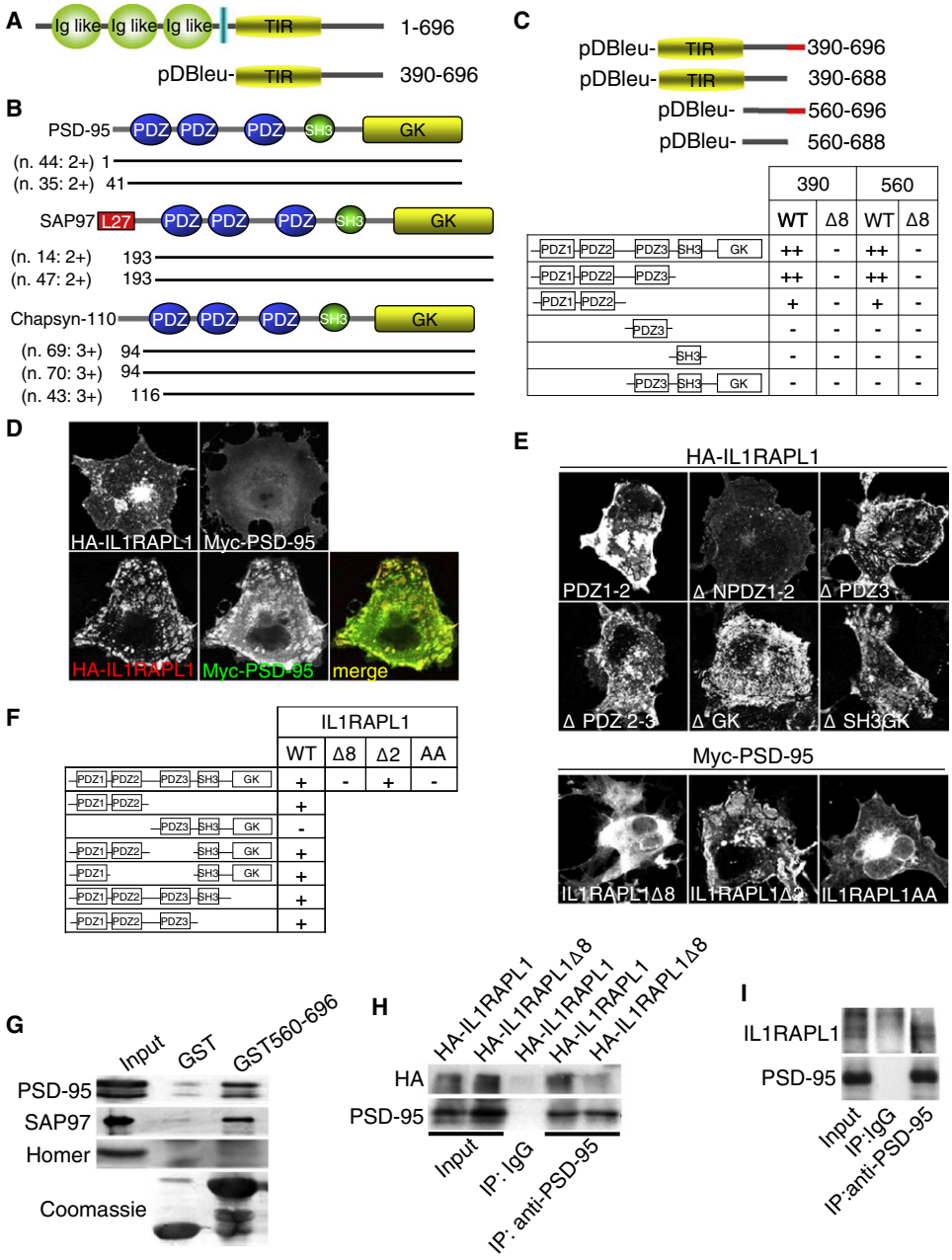

Figure 1. Characterization of IL1RAPL1/PSD-95 Interaction

(A) Schematic representation of IL1RAPL1 and the intracellular domain of IL1RAPL1 used as bait for the yeast two-hybrid screening.

(B) Results of the yeast two-hybrid screening with schematic representation of the positive clones of the MAGUK proteins: PSD-95, SAP-97, and chapsyn-110.

(C) Mapping of the PSD-95/IL1RAPL1 interaction by two-hybrid test.

(D–F) Coclustering assay in COS-7-transfected cell.

(G) Glutathione Sepharose (GST) pull-down experiment using a GST fusion protein with the C-terminal end of IL1RAPL1.

(H) Coimmunoprecipitation with protein extract from double-transfected COS-7 cells with PSD-95 plus a tagged version of IL1RAPL1 either full-length or deleted of the last 8 amino acids.

(I) Coimmunoprecipitation with neuronal extract.

using the entire intracellular region (aa 390–696, Figure 1A) as bait. Seven independent cDNA plasmids from positive clones encoded for the MAGUK proteins PSD-95, SAP-97, and chapsyn-110 (Figure 1B).

The interaction between IL1RAPL1 and PSD-95 was further studied by a yeast two-hybrid test with, as baits, the C terminus of IL1RAPL1 with or without the TIR domain (390–560 aa) and with or without the last 8 aa deleted (putative PDZ binding domain, aa 688–696). As prey, either the full-length or different domains of PSD-95 were used (PDZ1-PDZ2-PDZ3 [aa 1–403], PDZ1-PDZ2 [aa 1–256], PDZ3 [aa 303–403], SH3 [aa 418–508], PDZ3-SH3-GK [aa 303–724]) (Figure 1C). We found a putative PDZ binding domain within the last 8 aa of the C terminus of IL1RAPL1 that interacts

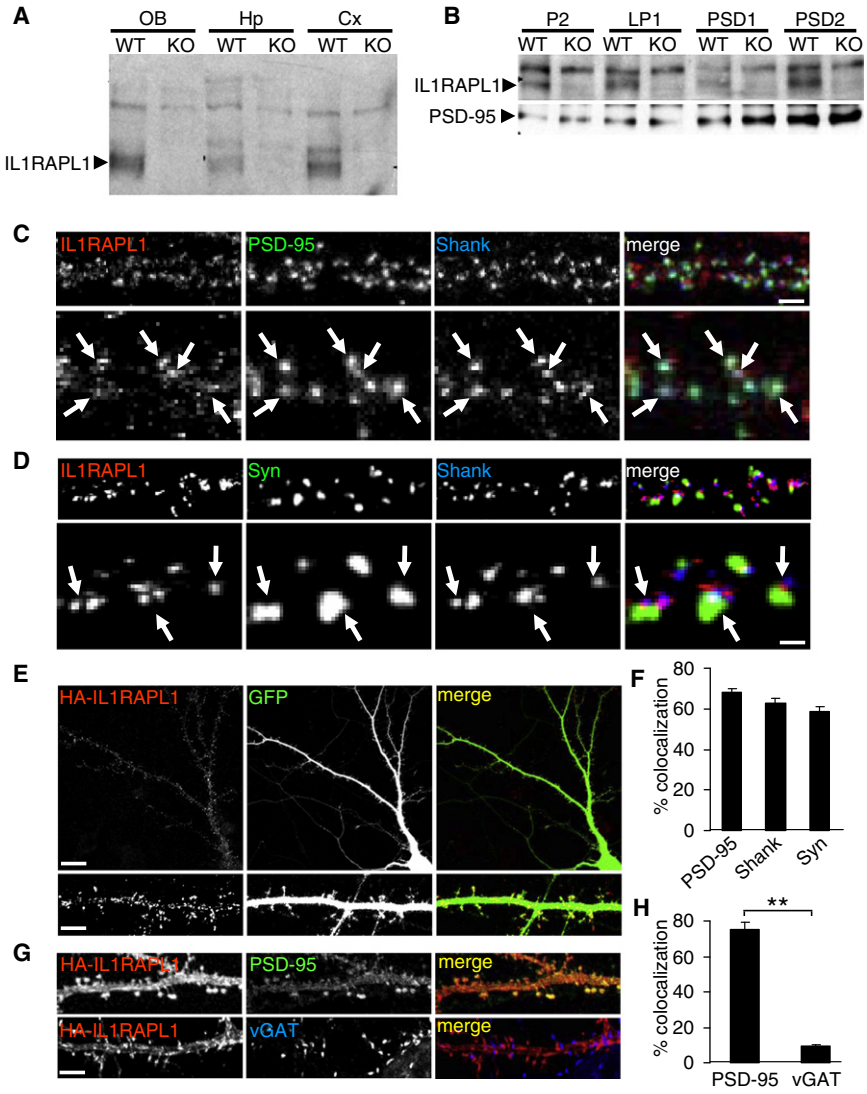

Figure 2. IL1RAPL1 Expression and Cellular Localization

(A) Homogenate from olfactory bulb (OB), hippocampus (Hp), and cortex (Cx) of wild-type (WT) and knockout (KO) mice were separated by SDS polyacrylamide gel electrophoresis (SDS-PAGE) and probed with IL1RAPL1 antibody (7.5 μg of protein per lane).

(B) IL1RAPL1 is present in synaptosomal fraction (P2) and synaptosomal membrane (LP1) and is enriched in postsynaptic density fractions (PSD-1 and PSD-2). Protein expression of PSD-95 is not affected by the absence of IL1RAPL1. Two different antibodies against IL1RAPL1 were used for (A) and (B) experiments: R&D antibody (A) and homemade antibody (B) (see Experimental Procedures).

(C) Immunostaining of rat hippocampal cultured neurons with antibody against IL1RAPL1 (K10), PSD-95, and Shank; bottom panels show higher magnification. Scale bars represent 3 μm (top) and 1.5 μm (bottom).

(D) Immunostaining of rat hippocampal cultured neurons with antibody against IL1RAPL1 (K10), synaptophysin, and Shank; bottom panels show higher magnification. Scale bars represent 3 μm (top) and 1.5 μm (bottom).

(E) Immunostaining of rat hippocampal cultured neurons double transfected with HA-IL1RAPL1 and GFP; bottom panels show higher magnification. Scale bars represent 10 μm and 5 μm.

(F) Quantification of the mean percent of colocalization (± standard error of the mean [SEM]) of endogenous IL1RAPL1 clusters with endogenous PSD-95, Shank, and synaptophysin clusters illustrated in (C) and (D); n = 10 neurons were used for the quantification.

(G) Rat hippocampal cultured neurons transfected with HA-IL1RAPL1 and immunolabeled with HA antibody and either PSD-95 or VGAT antibody. Scale bars represent 5 μm.

(H) Quantification of the mean percent of colocalization (±SEM) illustrated in (G) between HA-IL1RAPL1 and either PSD-95 or VGAT; n = 10 neurons were used for the quantification; **p < 0.01.

with PSD-95 via its first two PDZ domains (PDZ1 and PDZ2) (Figure 1C).

The interaction was confirmed with a transfected COS-7 coclustering assay. We found that wild-type (WT) HA-IL1RAPL1 forms intracellular coclusters with PSD-95 constructs (Figure 1D, bottom) containing at least one of the two first PDZ domains (Figures 1D–1F), whereas an IL1RAPL1 deleted mutant lacking the PSD-95 binding domain (HA-IL1RAPL1Δ8) does not. We noticed that the C terminus of IL1RAPL1 (TSISSVIW) contains a potential class I PDZ domain-binding motif, X-S/T-X-V [13]. This motif is localized in the C-terminal tail of IL1RAPL1 but contains two additional amino acids that are excluded from the classical motif sequence.

In order to investigate the role of these two amino acids of IL1RAPL1 in the interaction with PSD-95, we made two new constructs: HA-IL1RAPL1Δ2, with the last two C-terminal amino acids deleted, and HA-IL1RAPL1ΔAA, where the last two amino acids (IW) were replaced with two alanines (AA). When these mutants were cotransfected with myc-PSD-95, only the IL1RAPL1Δ2, and not the HA-IL1RAPL1ΔAA, was able to form clusters. This suggests that the last two amino acids of IL1-RAPL1 are also required for the interaction with PSD-95, and not in a classical type I PDZ motif sequence (Figures 1E and 1F).

Finally, the interaction between IL1RAPL1 and PSD-95 was biochemically proven by pull-down and immunoprecipitation experiments in transfected COS-7 cells and in vivo from neuronal protein extract. As shown in Figure 1G, the C-terminal tail of IL1RAPL1 was able to pull down PSD-95 and SAP-97 but not Homer from brain extract. In transfected COS-7 cells, IL1RAPL1 was coimmunoprecipitated with PSD-95, but the IL1RAPL1 with the last 8 aa deleted was not (Figure 1H). Lastly, IL1RAPL1 protein was specifically coimmunoprecipitated in brain extracts by a monoclonal anti-PSD-95 antibody (Figure 1I), showing that this interaction occurs in vivo.

IL1RAPL1 Is Localized in Postsynaptic Densities of Hippocampal Neurons

We then asked whether IL1RAPL1 is localized at the postsynapse site of the excitatory synapses as suggested by its interaction with PSD-95. It has been shown that *Il1rapl1* gene is expressed in adult mouse brain and cultured neurons [2]. Using a commercial antibody (see Experimental Procedures and legend of Figure 2A), we found that IL1RAPL1 is expressed in different regions of the brain, including the olfactory bulb, the cortex, and the hippocampus (Figure 2A). Using subcellular fractionation experiments, we showed that IL1RAPL1 is

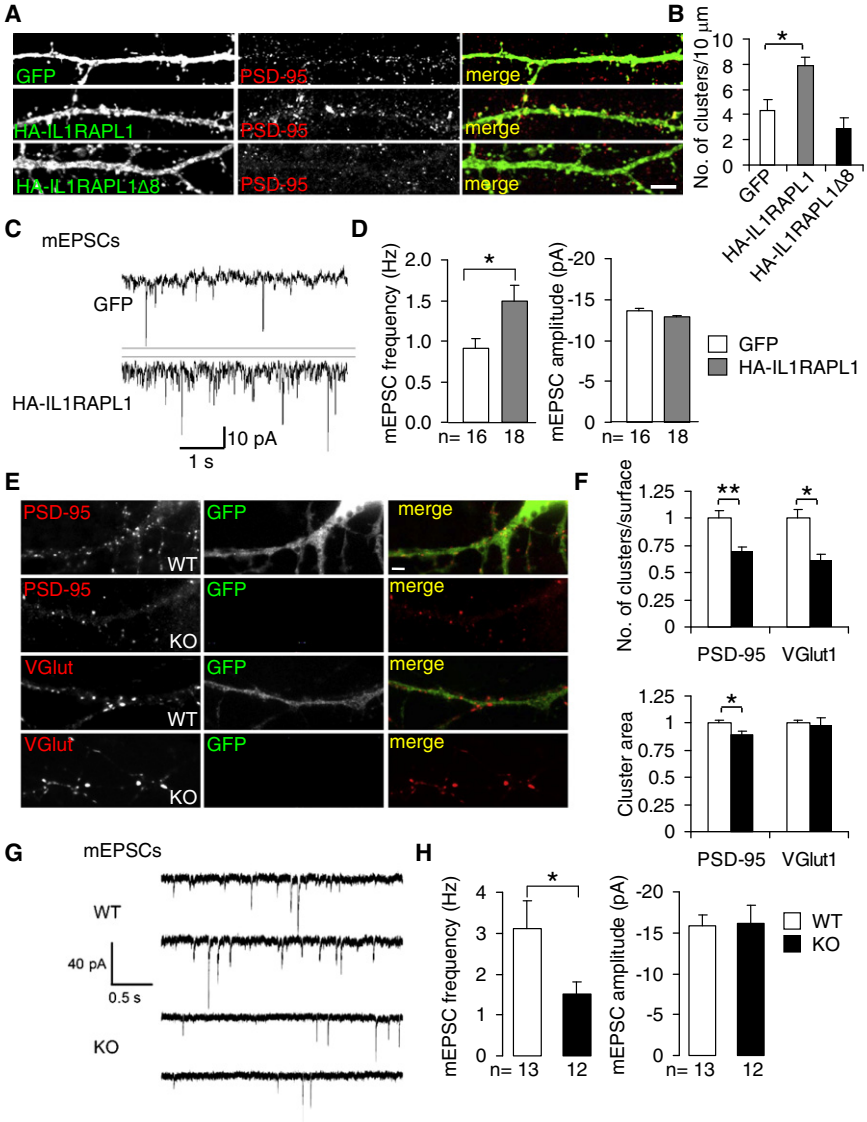

Figure 3. Consequences of Loss or Gain of IL1RAPL1 Function on Synapse in Cultured Hippocampal Neurons

(A) Rat hippocampal neurons were transfected with GFP or HA-tagged IL1RAPL1 either full-length or deleted of the last 8 amino acids and stained with PSD-95 and either GFP or HA antibody. Scale bar represents 10 μm.

(B) Quantification of number of PSD-95 clusters by unit of length in each condition; data are shown as mean ± SEM. *p < 0.05; n = 15 neurons for each transfected construct.

(C) Typical recording of miniature excitatory postsynaptic potentials (mEPSCs) of GFP or HA-IL1RAPL1 transfected neurons.

(D) Bar graphs of mean mEPSC frequency ± SEM (left) and mean mEPSC amplitude ± SEM (right); the number of recorded cells is indicated as n.

(E) Representative images of WT (GFP-positive) or KO (GFP-negative) hippocampal cocultured neurons costained for GFP (green) and PSD-95 or VGlut1 (red). Scale bar represents 3 μm.

(F) Quantitative analysis of the average cluster area or number of clusters per unit surface of PSD-95 and VGlut1 clusters. Data are shown as mean ± SEM normalized to WT. **p < 0.01, *p < 0.05; number of cells for PSD-95 cluster are WT = 42 and KO = 48; for VGlut1 cluster, WT = 22 and KO = 26.

(G) Typical recording of mEPSCs of IL1RAPL1 WT or KO neurons.

(H) Bar graphs of mean mEPSC frequency ± SEM (left) and mean mEPSC amplitude ± SEM (right); *p < 0.01; the number of recorded cells is indicated as n.

present in synaptosomal fraction and is enriched in postsynaptic density (PSD) fractions similarly to PSD-95 (Figure 2B). For this experiment, we used a different antibody [5] that recognizes two proteins with apparent molecular weight around 83 kDa. However, only the lower one is specific to IL1RAPL1, because it is absent in brain protein extracts from KO animals. Interestingly, loss of IL1RAPL1 does not affect the total amount of PSD-95 (Figure 2B; see also Figure S2B available online).

The synaptic subcellular localization of IL1RAPL1 was further studied by multiple-immunolabeling experiments in cultured hippocampal neurons with anti-IL1RAPL1 (K10, homemade antibody; see Experimental Procedures for details), anti-PSD-95, anti-Shank, and anti-synaptophysin antibodies. The endogenous IL1RAPL1 mostly colocalized with PSD-95 and Shank proteins (percent of IL1RAPL1 colocalization with PSD-95: 67.9% ± 2.2%; with Shank: 62.7% ± 2.6%) (Figures 2C and 2F), which are markers of excitatory postsynapses. Moreover, the triple staining of endogenous IL1RAPL1 with Shank and synaptophysin showed that IL1RAPL1 clusters are more overlapped with Shank clusters than with synaptophysin clusters (percent of IL1RAPL1 colocalization with synaptophysin: 58.8% ± 2.2%) (Figure 2D, arrowheads; Figure 2F). These results suggest that even if IL1RAPL1 is present at both sites of the synapse, it seems to be enriched in the postsynaptic compartment.

Immunostaining of transfected HA-IL1RAPL1 proteins shows a punctate staining in dendrites and dendritic spines (Figure 2E) (percent of dendritic spines labeled with HA-IL1RAPL1: 77.8% ± 3.6%). As shown in Figures 2G and 2H, transfected HA-IL1RAPL1 is highly colocalized with PSD-95 (percent of colocalization with PSD-95: 80.9% ± 3.3%) and only partially with vGAT (percent of colocalization with vGAT: 7.7% ± 1.3%). These data suggest that IL1RAPL1 is almost exclusively localized at the excitatory synapse and is enriched in the PSD.

IL1RAPL1 Affects PSD-95 Cluster Numbers in Neurons

The scaffold protein PSD-95 promotes the maturation and strengthening of excitatory synapses, functions that require proper localization of PSD-95 in the PSD. To investigate whether the interaction between IL1RAPL1 and PSD-95 had some effects on PSD-95 localization at synapse, we studied the consequences of HA-IL1RAPL1, HA-IL1RAPL1Δ8, or GFP overexpression in rat hippocampal neurons on PSD-95 clusters by immunolabeling.

As shown in Figures 3A and 3B (high magnification of dendrites and quantification of PSD-95 clusters), HA-IL1-RAPL1 overexpression in neurons increased PSD-95 cluster

density compared to GFP control, whereas overexpression of HA-IL1RAPL1Δ8 had no effect (number of PSD-95 clusters per 10 μm: neurons expressing GFP 4.3 ± 0.8; HA-IL1RAPL1 7.9 ± 0.7, $p < 0.05$; HA-IL1RAPL1Δ8 2.8 ± 0.9, $p = 0.22$ compared to GFP). Thus, IL1RAPL1 binds PSD-95 through its PDZ-binding domain, and in hippocampal cultured neurons, its overexpression promotes cluster formation of PSD-95. IL1RAPL1 overexpression in neurons also increased VGlut1 staining and dendritic spine number (but not the length or the width of the heads), suggesting that IL1RAPL1 overexpression increased excitatory synapse number, although both effects, presynaptic VGlut1 accumulation and increase of spine number, do not depend on IL1RAPL1 interaction with PSD-95 because they were also induced by the overexpression of IL1RAPL1Δ8 construct (VGlut1 staining mean intensity over transfected neurons normalized to untransfected neurons, percent increase: GFP 91.1% ± 17.8%; HA-IL1RAPL1 388.1% ± 33.9%, $p < 0.01$; HA-IL1RAPL1Δ8 404.5% ± 14.2%, $p < 0.01$ compared to GFP; dendritic spine number per 10 μm: GFP 4.3 ± 0.2; HA-IL1RAPL1 6.8 ± 0.3, $p < 0.05$; HA-IL1RAPL1Δ8 6.6 ± 0.2, $p < 0.05$ compared to GFP) (Figure S1). On the contrary, the overexpression of the construct deleted of most of the C-terminal region of IL1RAPL1 (IL1RAPL1ΔC) did not modify spine number (IL1RAPL1ΔC 3.6 ± 0.3, $p = 0.62$ compared to GFP) (Figures S1C and S1D). These data suggest that in hippocampal culture, IL1RAPL1 can regulate dendritic spine number independently of its interaction with PSD-95, but this requires the C-terminal domain.

In IL1RAPL1-overexpressing neurons, this increase of synapse number was associated with an increase of miniature excitatory postsynaptic potential (mEPSC) frequency (Figures 3C and 3D; mEPSC frequency of neurons expressing GFP: 0.9 ± 0.1 Hz; HA-IL1RAPL1: 1.5 ± 0.2 Hz, $p < 0.5$), whereas no modification of mEPSC amplitude was observed (Figures 3C and 3D; mEPSC amplitude of neurons expressing GFP: 13.6 ± 0.3 pA; HA-IL1RAPL1: 12.8 ± 0.3 pA; $p = 0.07$). These results indicate that overexpression of IL1RAPL1 increases excitatory synapse number and that these synapses are functional.

In order to evaluate the consequences of the loss of IL1RAPL1 on excitatory synapses, we studied pre- and postsynaptic markers in IL1RAPL1 KO versus WT hippocampal cultured neurons. To avoid possible differences deriving from heterogeneity between independent IL1RAPL1 KO and WT cultures, we used a cocultured system in which only WT neurons, and not KO neurons, express the GFP protein (see Experimental Procedures for details). Intriguingly, we found that loss of IL1RAPL1 in cultured hippocampal neurons led to a 25% decrease in the density of PSD-95 and VGlut1 clusters compared to WT (PSD-95 cluster density normalized to WT neurons: WT = 1 ± 0.08, KO = 0.73 ± 0.07, $p < 0.01$; VGlut1: WT = 1 ± 0.08, KO = 0.76 ± 0.07, $p < 0.05$) (Figures 3E and 3F). This reduction in the density of excitatory synapses is associated to a slight but significant reduction of the PSD-95 cluster area without affecting that of VGlut1 clusters (PSD-95 cluster mean area normalized to WT: WT = 1 ± 0.05, KO = 0.86 ± 0.04, $p < 0.05$; VGlut1 cluster: WT = 1 ± 0.05, KO = 0.92 ± 0.04, $p = 0.20$) (Figure 3F). In addition, we also confirmed these results in cultured cortical neurons (data not shown). Altogether, these data indicate that the loss of IL1RAPL1 leads to a reduction of excitatory synapse density that is paralleled by a specific decrease of PSD-95 localization at the remaining synapses. The reduction of excitatory synapse number in IL1RAPL1 KO neurons is associated with a reduction of mEPSC frequency (Figures 3G and 3H; mEPSC frequency of WT: 3.1 ± 0.7 Hz; KO: 1.5 ± 0.3 Hz; $p < 0.05$). The amplitude of mEPSC is not modified by IL1RAPL1 loss of function (Figures 3G and 3H; mEPSC amplitude of WT: 15.9 ± 1.3 pA; KO: 16.2 ± 2.1 pA; $p = 0.683$). In cultured IL1RAPL1 KO neurons, the reduction of PSD-95 localization to the remaining synapse does not seem to have an effect on basal synaptic transmission because the amplitude and the kinetics of miniature EPSCs (data not shown) is unchanged compared to WT cultured neurons.

IL1RAPL1 Promotes PSD-95 Phosphorylation and Its Recruitment to Synapses

It has been reported that overexpression of IL1RAPL1 in human embryonic kidney (HEK) cells stimulates JNK pathway [10]. We first confirmed these results using PC12 cell lines stably expressing IL1RAPL1 (data not shown) [5]. Because the phosphorylation level of Ser-295-PSD-95 by JNK affects its synaptic localization [11], we then asked whether the mislocalization of PSD-95 observed in cultured KO neurons could be associated with a deregulation of JNK pathway. To address this question, we first looked at phosphorylation level of PSD-95 in hippocampal neurons overexpressing β-galactosidase, HA-IL1RAPL1, or HA-IL1RAPL1Δ8 (Figure 4A). Overexpression of HA-IL1RAPL1 induced a significant increase of PSD-95 phosphorylation on serine 295, whereas overexpression of IL1RAPL1Δ8 had no effect (intensity ratio pPSD-95/PSD-95: β-galactosidase: 0.5 ± 0.10; HA-IL1RAPL1: 0.85 ± 0.06; $p < 0.01$; HA-IL1RAPL1Δ8: 0.6 ± 0.06, not significant compared to β-galactosidase) (Figures 4A and 4B). Thus, IL1RAPL1 overexpression in neurons is able to increase PSD-95 phosphorylation (on Ser-295), and this effect is dependent on its interaction with PSD-95.

We next examined the consequence of loss of function of IL1RAPL1 on the phosphorylation levels of both PSD-95 and JNK, which phosphorylates PSD-95 on Ser-295 amino acid residue. We first used total protein extracts from WT or KO neuronal cultures at 21 days in vitro (DIV) and monitored the phosphorylation levels of JNK and PSD-95 via western blot experiments. Opposite to data from IL1RAPL1 overexpression, we found that, in basal conditions (nontreated, NT), the phosphorylation level of PSD-95 was decreased by 30% in cultured IL1RAPL1-KO neurons (phosphorylation level of PSD-95: WT = 1.00 ± 0.05, KO = 0.72 ± 0.02; $p < 0.001$) (Figures 4C and 4E). Similarly, we observed a strong decrease of the phosphorylation level of JNK in KO cultured neurons compared to WT (phosphorylation level of JNK: WT = 1.00 ± 0.05, KO = 0.53 ± 0.06; $p < 0.001$) (Figures 4D and 4F). Given that IL1RAPL1 deficit does not change the total level of both JNK and PSD-95 protein (Figure S2B), these results show that loss of IL1RAPL1 decreases JNK activity and consequently leads to a reduction of PSD-95 phosphorylation at the S295 residue.

It has been recently shown that synaptic activity regulates phosphorylation levels of PSD-95 in neuronal cultures [11]. Thus, we investigated whether IL1RAPL1-mediated phosphorylation is activity dependent. This was done by studying whether the deficit in JNK activity in IL1RAPL1 KO neurons, and consequently of phosphorylation level of PSD-95, were sensitive to a blockade of neuronal network activity by tetrodotoxin (TTX). As previously shown by Kim et al. [11], the phosphorylation level of PSD-95 in cultured WT neurons is increased after TTX treatment, whereas there is no significant effect on JNK activity. This suggests that neuronal network activity regulates PSD-95 phosphorylation through control of

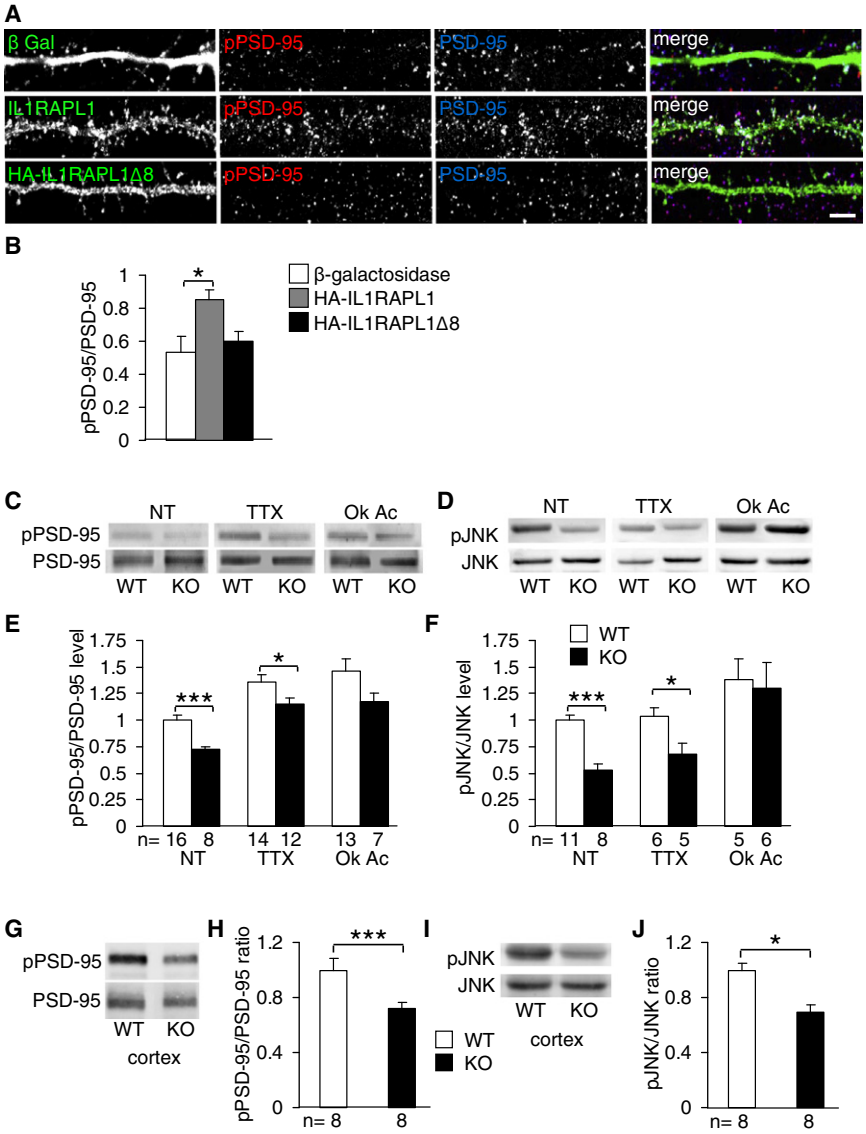

Figure 4. PSD-95 Phosphorylation and JNK Pathway

(A) Immunostaining with pPSD-95 and PSD-95 antibody of rat hippocampal neurons transfected with either β-galactosidase or HA-IL1RAPL1, full-length or deleted of the last 8 amino acids.

(B) Quantitative analysis of pPSD-95 cluster intensity normalized to PSD-95, representative of PSD-95 phosphorylation on Ser-295; data are shown as mean of the ratio of cluster pixel intensity ± SEM; *p < 0.01; n = 20 neurons for each construct. Scale bar represents 10 μm.

(C–F) KO or WT cultured neurons were treated or not treated (NT) for 2.5 hr with tetrodotoxin (TTX) or okadaic acid (Ok Ac).

(C and D) Representative immunoblots of PSD-95 (C) or c-Jun terminal kinase (JNK) (D) phosphorylation level in each condition for both genotypes.

(E and F) Quantification of PSD-95 (E) and JNK (F) phosphorylation level of experiments performed as shown in (G) and (H). Data are shown as mean of pJNK/JNK or pPSD-95/PSD-95 level ± SEM normalized to untreated WT. ***p < 0.001, *p < 0.05; the number of experiments is indicated as n.

(G–J) Phosphorylation level of JNK and PSD-95 in KO and WT cortices. Total protein extract from WT or KO cortices was separated by SDS-PAGE and probed with pPSD-95 (G) or pJNK (I) antibody, then stripped and reprobed with PSD-95 or JNK antibody, respectively. Quantification of PSD-95 (H) and JNK (J) phosphorylation level of experiments was performed as shown in (C) and (E). Data are shown as mean of pPSD-95/PSD-95 or pJNK/JNK level ± SEM normalized to WT. ***p < 0.001, *p < 0.05; the number of experiments is indicated as n.

phosphatase activities (Figures 4C–4F; Figure S2A). Similarly with WT, TTX induced PSD-95 phosphorylation in KO without any effect on JNK activity, whereas differences in PSD-95 and JNK phosphorylation levels were still present between the two genotypes (phosphorylation level of JNK: WT_{TTX} = 1.04 ± 0.09, KO_{TTX} = 0.68 ± 0.10, p < 0.05; PSD-95: WT_{TTX} = 1.36 ± 0.07, KO_{TTX} = 1.15 ± 0.06, p < 0.05) (Figures 4C–4F; Figure S2A). These results show that, in KO neurons, there is a constitutive deficit of JNK activity and PSD-95 phosphorylation, and also that regulation of PSD-95 phosphorylation level by synaptic activity is independent of IL1RAPL1.

Because both JNK and PSD-95 are dephosphorylated by PP1 and PP2A phosphatases [11, 14], we treated KO and WT neuronal cultures with the PP1 and PP2A phosphatase inhibitor okadaic acid (OA) for 2.5 hr before protein extraction. As shown in Figures 4C and 4E and in agreement with published data [11], inhibition of PP1 and PP2A in WT neurons induced an increase of JNK activity and consequently of the phosphorylation level of PSD-95 (Figures 4C–4F; Figure S2A). Interestingly, inhibition of PP1 and PP2A in KO neurons also increased the phosphorylation levels of JNK and PSD-95 and partially compensated the differences between genotypes (phosphorylation level of JNK: $WT_{OA.}$ = 1.39 ± 0.19, $KO_{OA.}$ = 1.3 ± 0.25, p = 0.79; PSD-95: $WT_{OA.}$ = 1.46 ± 0.12, $KO_{OA.}$ = 1.17 ± 0.08, p = 0.11) (Figures 4D and 4F; Figure S2A).

Finally, we used total protein cortical extracts from WT and KO animals to study the in vivo role of IL1RAPL1 in regulation of JNK and PSD-95 phosphorylations. Similarly to our in vitro data, we found a 30% reduction of PSD-95 phosphorylation at Ser-295 residue (PSD-95 phosphorylation level: WT = 1.00 ± 0.05, KO = 0.69 ± 0.05, p < 0.001) (Figures 4G and 4H) in the cerebral cortex of IL1RAPL1 null mutants. This decrease was paralleled by a similar decrease in JNK phosphorylation level (phosphorylation level of JNK: WT = 1.00 ± 0.09, KO = 0.72 ± 0.03, p < 0.05) (Figures 4I and 4J). In conclusion, we show that loss of IL1RAPL1 constitutively reduces JNK activity and PSD-95 phosphorylation in the brain and that treatment with the phosphatase inhibitor OA partially restores these deficits.

IL1RAPL1 Is Important for the Formation of Excitatory Synapses In Vivo

A significant reduction of excitatory synapse numbers produced by in vitro loss of IL1RAPL1 function suggested the investigation of the role of IL1RAPL1 protein in the organization of neural circuits in vivo. To address this question, we analyzed the brain of IL1RAPL1 KO mice using both confocal and electron microscopy. First, we analyzed the structural organization of the hippocampus and found no obvious

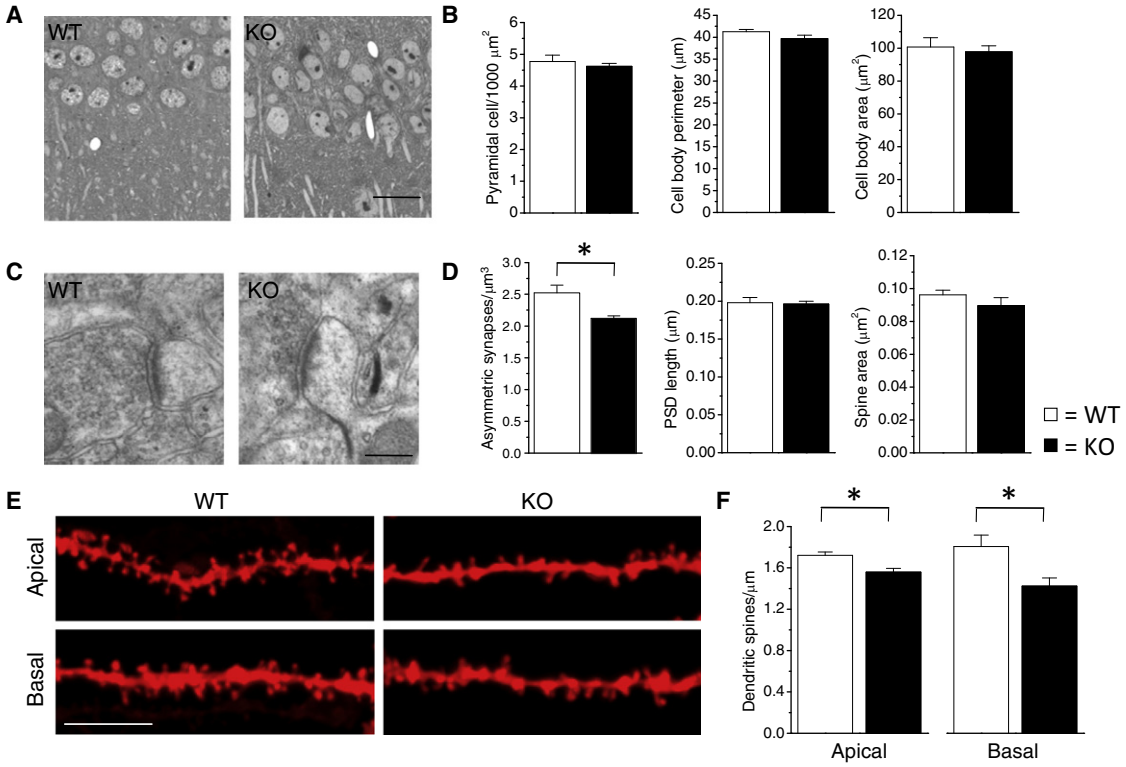

Figure 5. Structural Organization of CA3-CA1 Synapses in the Hippocampus of IL1RAPL1 KO Mice

(A) Representative semithin section micrographs showing CA1 pyramidal neurons of IL1RAPL1 KO and WT littermate mice; scale bar represents 50 μm.

(B) Quantitative analysis of CA1 pyramidal cell density, cell body perimeter, and area. Data are shown as mean ± SEM; n = 3 for each genotype.

(C) Representative electron micrographs of asymmetric axospinous contact in the striatum radiatum of the CA1 area of hippocampus of IL1RAPL1 KO and WT animals; scale bar represents 200 nm.

(D) Quantitative analysis of the number per unit of volume and of the average of postsynaptic density (PSD) length and dendritic spine area of these contacts. Data are shown as mean ± SEM; *p < 0.05; n = 3 for each genotype.

(E) DiOlistic fluorescent labeling of basal and apical dendrites of the hippocampus CA1 pyramidal neurons of IL1RAPL1 KO and WT mice; scale bar represents 5 μm.

(F) Quantitative analysis of dendritic spine density of apical or basal dendrites. Data are shown as mean ± SEM; *p < 0.05; n = 4 for each genotype.

neurocytological abnormalities (Figure 5A). Indeed, CA1 pyramidal cell density (WT: 4.7 ± 0.2 cells/1000 μm^2; KO: 4.6 ± 0.1 cells/1000 μm^2), cell body perimeter (WT: 41.2 ± 5.2 μm; KO: 39.7 ± 7.7 μm), and cell body area (WT: 100.7 ± 5.6 μm^2; KO: 97.8 ± 3.6 μm^2) were unchanged in IL1RAPL1 KO mice when compared to WT animals (Figures 5A and 5B). Next, we calculated the density of asymmetric axospinous contacts in the stratum radiatum of the CA1 area of the hippocampus (Figures 5C and 5D) using stereology and electron microscopy. This analysis revealed that *Il1rapl1* null mutation produced a significant decrease in the number of asymmetric synapses in this area (WT: 2.4 ± 0.07 contacts/μm^3; KO: 1.8 ± 0.15 contacts/μm^3, $p < 0.05$). Interestingly, the reduction of excitatory synapses was paralleled by a significant decrease in the number of postsynaptic dendritic spines protruding from secondary and tertiary dendritic segments of CA1 pyramidal neurons (Figures 5E and 5F). The number of dendritic spines identified with diolistic fluorescent labeling was reduced in IL1RAPL1 KO mice on both apical and basal dendrites of CA1 pyramidal neurons (apical: WT: 1.7 ± 0.03 contacts/μm; KO: 1.5 ± 0.03 contacts/μm, $p < 0.05$; basal: WT: 1.7 ± 0.1 contacts/μm; KO: 1.3 ± 0.07 contacts/μm, $p < 0.05$) (Figures 5E and 5F). Similarly, we also observed a reduction of spine density on the dendritic branches of layer V pyramidal neurons, although the decrease was not significant because of higher variability in cortex compared to hippocampus (data not shown).

Although the deletion of *Il1rapl1* produced significant alterations in the number of excitatory synapses, it did not affect the architecture of these contacts. Electron microscopy analysis of the length of the PSD and of the spine cross-section area (Figure 5D) showed that there was no change in KO animals when compared to WT mice (PSD length: WT: 0.19 ± 0.07 μm; KO: 0.19 ± 0.03 μm; spine area: WT: 0.96 ± 0.03 μm^2; KO: 0.89 ± 0.05 μm^2) (Figure 5D). Similarly, spine neck length was not modified in IL1RAPL1 KO animals with respect to WT mice (data not shown). Interestingly, presynaptic structures also seemed normal in mutant mice. The electron microscopy analysis of presynaptic terminal area did not show significant differences in KO animals when compared to WT mice (WT: 0.15 ± 0.01 μm^2; KO: 0.19 ± 0.006 μm^2; Figure S4A). Moreover, no differences were found in the density of total synaptic vesicles (WT: 367.9 ± 19.8 vesicles/μm^2; KO 360.4 ± 30.8 vesicles/μm^2) as well as docked synaptic vesicles (WT: 27.07 ± 0.88 vesicles/μm of active zone; KO: 25.67 ± 1.4 vesicles/μm of active zone) between genotypes (Figure S4A). Thus, these data indicate that *Il1rapl1* null mutation in vivo induces a reduction in excitatory contact density but does not seem to alter synaptic morphology of the remaining synapses.

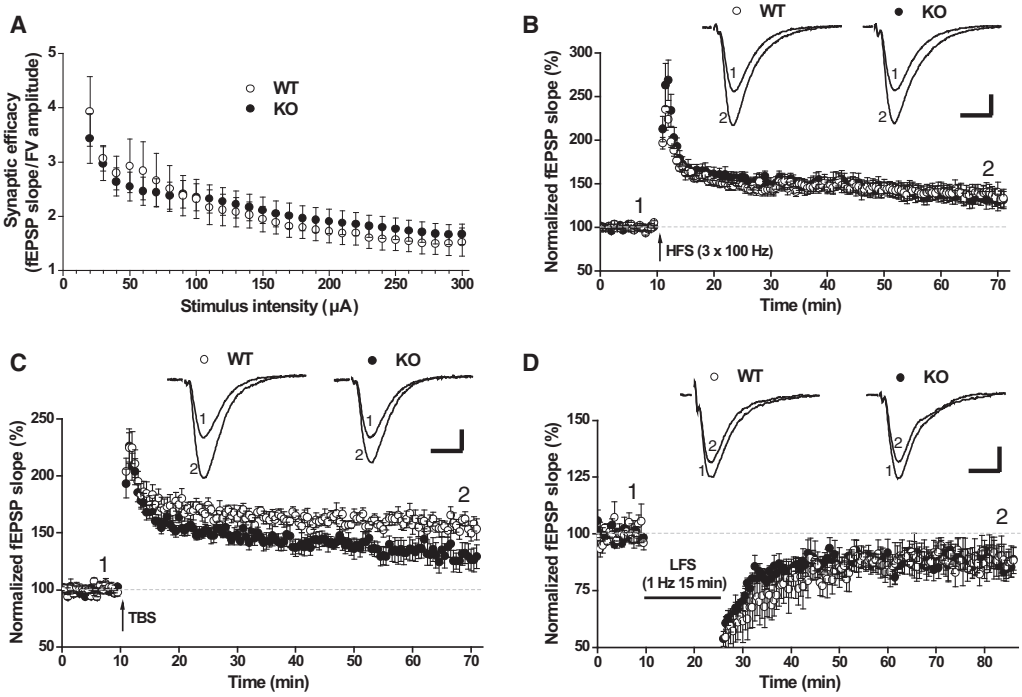

Figure 6. Synaptic Transmission and Long-Term Plasticity at SC-CA1 Synapses of the Hippocampus of IL1RAPL1 KO Mice

(A) Synaptic efficacy of hippocampal responses recorded by stimulating Schaffer collateral at intensities ranging from 20 to 300 μA was similar in IL1RAPL1 KO mice (open circles, n = 12 slices from 4 mice) and WT mice (closed circles, n = 11 slices from 4 mice).

(B) Long-term potentiation induced by high-frequency stimulation (HFS, arrow) was identical in KO (n = 8 slices from 4 mice) and in WT (n = 9 slices from 4 mice) animals.

(C) Long-term potentiation (LTP) induced by theta-burst stimulation (TBS, arrow) was significantly reduced in IL1RAPL1 mutant mice compared to WT ($p < 0.05$, analysis of variance; LTP values measured at minutes 55–60 after TBS; n = 8 slices from 3 mice both for KOs and WTs).

(D) Long-term depression (LTD) was not affected by IL1RAPL1 deletion: no differences in the magnitude of the responses were observed between KO (n = 7 slices from 3 mice) and WT (n = 5 slices from 3 mice) at any moment after low-frequency stimulation (LFS, indicated by horizontal black line). Insets above (B), (C), and (D) show averaged field postsynaptic potentials from three consecutive traces taken at the time points indicated by the numbers. Calibration bars represent 10 ms (horizontal) and 0.5 mV (vertical). All data are presented as means ± SEM of the indicated number of experiments.

Next, we investigated whether *Il1rapl1* null mutation could also affect the number and organization of inhibitory synapses in the hippocampus by using immunogold labeling and electron microscopy. Qualitative analysis of GABA-positive axon terminals making symmetric synapses on the cell soma of CA1 pyramidal neurons did not reveal major ultrastructural abnormalities (Figures S5A and S5C). Interestingly, the density of perisomatic GABAergic synapses was not altered in IL1RAPL1 KO mice (number of contacts per membrane length WT: 0.17 ± 0.02 N/10 μm of membrane; KO: 0.18 ± 0.01 N/10 μm of membrane; Figure S5B).The density of immunogold particles decorating GABAergic axon terminals was also not altered (WT: 214 ± 20 N/nm^2; KO: 210 ± 12 N/nm^2; Figure S5C). Altogether, these data show that IL1RAPL1 deficit does not affect inhibitory synapses in the CA1 region of hippocampus.

Long-Term Potentiation Is Altered in IL1RAPL1 KO Mice

To explore the physiological consequences of the structural modifications induced by *Il1rapl1* loss-of-function mutation, we investigated basal synaptic transmission at SC-CA1 pathway in hippocampal acute slices of WT and IL1RAPL1 KO mice. Synaptic efficacy, calculated as the ratio between the slope of the field postsynaptic potentials (fEPSPs) and the amplitude of the fiber volley, was not different between KO and WT mice at any of the stimulus intensities tested (Figure 6A). Because field potential method could be not sensitive enough to detect small changes in basal synaptic transmission, we used patch-clamp and minimal stimulation protocol to test whether the reduction of spine in IL1RAPL1 KO hippocampus affects neurotransmission at SC-CA1 synapses (Figures S3A–S3C). With minimal stimulation, failure and success events have the same distribution in IL1RAPL1 KO and WT. Deficit in IL1RAPL1 led to a small but not significant reduction of minimal evoked EPSC (meEPSC) amplitude (meEPSCs WT: −13.6 ± 1.8 pA, KO: −12.7 ± 0.8 pA, p = 0.62). In input-output function, IL1RAPL1 KO CA1 pyramidal cells have weaker responses than WT, but the difference is once again not significant (eEPSC at 300 μA of stimulation: WT: −313 ± 47 pA, KO: −294 ± 67 pA, p = 0.82) (Figures S3D and S3E). Together with field recording result, these data suggest that the reduction of around 20% of excitatory synapse number in the hippocampal CA1 region of IL1RAPL1 KO mice has no noticeable effect on basal neurotransmission.

To explore presynaptic plasticity, we measured paired-pulse facilitation (PPF) ratios, tested with interstimulus intervals (ISI) ranging from 10 to 300 ms. PPF ratios were not statistically different between KO and WT animals at any of the ISI tested (Figure S4B), showing that in this region of hippocampus, presynaptic short-term plasticity is not altered by IL1RAPL1 deletion.

Next, we investigated several forms of long-term synaptic plasticity at hippocampal SC-CA1 synapses. Long-term potentiation (LTP) elicited by high-frequency stimulation (HFS) was unchanged in IL1RAPL1 KO animals: the increase

in the magnitude of synaptic responses was identical in WT and mutants for at least 60 min following the delivery of the HFS (Figure 6B). LTP values measured at minutes 55–60 after HFS were 139.13% ± 9.04% for WT mice and 133.40% ± 8.94% for KO ($p = 0.66$, analysis of variance [ANOVA]). Interestingly, LTP was slightly but significantly impaired (Figure 6C) in slices from KO mice when it was elicited via a paradigm of theta-burst stimulation (TBS-LTP), which is thought to mimic the firing patterns observed in the hippocampus during behavioral learning in animals in vivo [15]. Although the magnitude of synaptic responses recorded during the first minutes after TBS was similar, differences between the two genotypes started to appear at minutes 15–20 (136.61% ± 8.99% in KO mice versus 166.46% ± 5.28% in WTs, $p < 0.05$, ANOVA), and LTP values, measured 1 hr after TBS (minutes 55–60), were significantly reduced in KO mice (129.05% ± 9.52%) with respect to WTs (156.86% ± 5.84%; $p < 0.05$, ANOVA). Application of low-frequency stimulation (LFS) protocol to the SC of WT mice caused a reduction in the size of synaptic responses recorded in CA1 stratum radiatum. This LFS protocol, when applied to the SC of KO mice, produced a similar reduction (WT: 88.74% ± 5.92%; KO: 88.06% ± 4.89%; $p = 0.93$, ANOVA). Thus, these data indicate that an absence of IL1RAPL1 may produce stimulus-specific impairments in long-term synaptic plasticity affecting the consolidation and maintenance phases of LTP.

Discussion

In this study, we showed that the MR-related protein IL1RAPL1 is present in the PSD of excitatory synapses where it interacts with PSD-95 through a noncanonical PDZ-binding motif. Using transfection experiments in hippocampal neurons, we demonstrated that the PDZ-binding motif of IL1RAPL1 is involved in the regulation of PSD-95 localization in synapses. IL1RAPL1 overexpression in neurons increases the number of PSD-95 clusters in dendritic spines, whereas deletion of the PDZ-binding motif abolishes this effect. Deletion of IL1RAPL1 leads to a decrease of excitatory synapse number both in cultured neurons and in the brain of mutant animals and abnormal long-lasting synaptic plasticity. These results suggest an involvement of IL1RAPL1 in promoting the formation or in the stabilization of excitatory synapses and in the correct function of these contacts.

In IL1RAPL1 KO neurons, we found a decrease in JNK activity and consequently in the phosphorylation level of the Ser-295 of PSD-95 leading to a reduction of PSD-95 localization at the synapse. How IL1RAPL1 can regulate JNK activity is still not clear. Because Rac1 has been described as an upstream regulator of JNK activity in neurons [11], it is possible that Rac1 activity is altered by IL1RAPL1 deletion. Alternatively, Wnt5 signaling has also been involved in regulating JNK pathway and PSD-95 localization [16], suggesting a complex regulation of JNK/PSD-95 pathway in neurons.

We found that the deficit in JNK activity and in PSD-95 phosphorylation is partially rescued in IL1RAPL1 KO neurons treated by okadaic acid, an inhibitor of PP1 and PP2A phosphatases, whereas inhibition of neuronal network activity by TTX similarly increases PSD-95 phosphorylation level independently of the genotype. These results lead to at least two hypotheses: IL1RAPL1 enhances JNK activity as suggested by IL1RAPL1 overexpression in HEK cells [10] and/or it can inhibit PP1 and PP2A phosphatase activity that regulates JNK activity and PSD-95 phosphorylation (Figure S6). In both hypotheses, IL1RAPL1 is likely to locally regulate JNK and modulate the phosphorylation of the scaffolding protein PSD-95 at the synapse in response to a yet-unknown signal. JNK pathways have also been involved in axonal growth and microtubule dynamics through regulation of phosphorylation states of microtubule-associated proteins such as MAP-2 or doublecortin [17, 18]. In either loss- or gain-of-function approaches, we did not find any evidence of neuronal migration or morphogenesis defects. This argument is in favor of the local regulation of JNK pathway by IL1RAPL1 at the synapse rather than a more general cell-wide effect.

In vitro as well as in vivo, we showed that increase or loss of IL1RAPL1 function leads to an increase or decrease of excitatory synapse number, respectively. The overexpression of IL1RAPL1 increases the number of dendritic spines without changing the morphology. In agreement with these data, in IL1RAPL1 KO mice, the reduction in number of excitatory synapses in pyramidal neurons of the CA1 region of hippocampus is not associated with abnormal organization of the pre- and the postsynaptic compartment, indicating that the remaining synapses are not affected by loss of IL1RAPL1 at the structural level.

As previously shown [19], IL1RAPL1 is not expressed in the CA3 region of the hippocampus. This suggests that the analysis of the SC-CA1 synapses in IL1RAPL1 KO mice should give us clues about the postsynaptic role of IL1RAPL1 and, eventually, the secondary consequences on the presynaptic compartment of postsynaptic deficit in IL1RAPL1 expression. At the SC-CA1 synapse, neither basal synaptic transmission nor presynaptic short-term plasticity is affected by loss of IL1RAPL1, suggesting that postsynaptic loss of IL1RAPL1 has no major effect on the presynaptic compartment.

Long-term synaptic plasticity in the hippocampus has been shown to be a substrate for memory and learning. Here we found that only theta-burst-induced LTP is impaired in IL1RAPL1 KO mice, whereas HFS-induced LTP is normal. Interestingly, our data show that theta-burst-induced LTP appears to be negatively affected by IL1RAPL1 deletion as soon as 15–20 min after theta-burst stimulation and that LTP deficit becomes even more evident in the next 40 min of LTP. The relevance of HFS- and theta-burst-induced LTP at this synapse has been discussed by Albensi and colleagues [20]: theta-burst-induced LTP is physiologically closer to what occurs in the hippocampus during episodes of learning and memory in living animals, and consequently, from a pathophysiological standpoint, deficits in theta-burst-induced LTP are potentially more relevant than deficits in HFS-induced LTP. Moreover, Boda and colleagues [21] showed that, among other genes involved in MR, expression level of *Il1rapl1* is specifically increased following theta-burst-induced LTP at SC-CA1 synapse in mice, suggesting that *Il1rapl1* expression could be required for further positively regulating theta-burst-induced LTP. At the molecular level, it is known that theta-burst- and HFS-induced LTP do not involve the same VGCC and Ca^{2+} store [22]. We have previously shown that IL1RAPL1 interacts with NCS-1 [5] and, through this interaction, regulates N-type VGCC activity in PC12 cells [6]. These previous results showed an involvement of IL1RAPL1 in exocytosis, suggesting a possible role of this protein in the release of neurotransmitter at the synapse. However, at present, because NCS-1 [23] and VGCC [24] are both present in the postsynaptic compartment, we cannot exclude a deregulation of NCS-1/VGCC pathway in the postsynaptic compartment carrying unknown consequences on LTP in the

IL1RAPL1 KO mice. On the other hand, the deficit in theta-burst-induced LTP in IL1RAPL1 KO mice could be due to a decrease of PSD-95 synaptic content, with critical consequences on glutamate receptor trafficking. In apparent contrast with our results, mutant mice for PSD-95 show enhanced LTP at different frequencies of synaptic stimulation [25]. However, a plausible explanation for this discrepancy is that in this mouse model there is a specific loss of PSD-95. In contrast, IL1RAPL1 deletion may alter the distribution and function of the other interacting postsynaptic MAGUK proteins (i.e., SAP-97 and chapsyn-110). Importantly, whereas PSD-95 mutants showed no changes in morphology or number of synaptic structures, we show that IL1RAPL deletion leads to a decreased number of dendritic spines and asymmetric synapses in the stratum radiatum of the CA1 region of the hippocampus.

In conclusion, the finding of PSD-95 as a novel partner of IL1RAPL1 and the implication of the JNK/PSD-95 pathway in the IL1RAPL1 KO phenotype disclose a novel pathophysiological mechanism for MR associated with IL1RAPL1 mutations.

Experimental Procedures

Animals

IL1RAPL1 KO and B6C3F1-Tg(CAG-EGFP)CX transgenic mice have been described previously [12, 26]. C57BL/6N mice were purchased from Charles River. Animals were weaned at 4 weeks and housed two to four per cage by sex and litter regardless of the genotype under standard conditions, with food and water available ad libitum. Experiments were performed in accordance with the European Communities Council Directive (86/809/EEC) regarding the care and use of animals for experimental procedures and were approved by the local ethical committee.

Yeast Two-Hybrid Screening and cDNA Constructs

A fragment corresponding to the intracellular domain of IL1RAPL1 (aa 390–696) was cloned in pDBLeu in frame with GAL4 binding domain, used as a bait for screening a human fetal brain cDNA library (ProQuest Pre-made cDNA Libraries), and cloned in pPC86 vector. Positive colonies were selected for the ability to grow on plate lacking amino acids Tryptophane, Leucine, and Histidine but containing 10 mM 3AT and to be positive for β-galactosidase activity (*LacZ* test). cDNA plasmids from positive clones were recovered via *E. coli* DH5α plated on Amp^R and then sequenced.

Original, full-length cDNA construct of *IL1RAPL1* was obtained by J. Sims (Amgen) (AF284435, aa 1–696). HA-tagged or deletion constructs were prepared with standard molecular biology techniques: for all HA-IL1RAPL1-tagged constructs, tag was inserted between residues 24 and 25 of IL1RAPL1. This construct was used as template for all the IL1RAPL1 mutant constructs. For yeast two-hybrid screening, the indicated residues of IL1RAPL1 were subcloned into pDBLeu vector (baits), and different domains of PSD-95 (PDZ1–2, aa 1–256; SH3, aa 418–508; PDZ3SH3GK, aa 303–724; PDZ3, aa 303–403, full length of PSD-95) were subcloned into pPC86 vector (preys). For pull-down assay, aa 560–696 and aa 560–688 of IL1RAPL1 were subcloned into pGEX-4T vector.

Biochemistry Experiments: GST Pull-Down and Immunoprecipitation

Glutathione Sepharose (GST) fusion proteins were prepared in *E. coli* BL21 strain and purified according to standard procedures. Transfected human embryonic kidney 293T (HEK293T) cells were lysed with lysis buffer (50 mM TRIS-HCl [pH 7.4], 150 mM NaCl, 1 mM EDTA, 1% NP40, 0.5% deoxicholate). Cellular lysates were then incubated with 30 μg of GST fusion protein immobilized on GST 4B beads (GE Healthcare) for 3 hr at 4°C, washed extensively five times in the lysis buffer, and resuspended in 25 μl of 3× SDS sample buffer. GST alone was used as control. Samples were separated by SDS polyacrylamide gel electrophoresis (SDS-PAGE) followed by western blotting.

For the coimmunoprecipitation, samples (100 μg proteins) were incubated overnight at 4°C with antibodies (antibody dilution 1:200) in buffer A containing 200 mM NaCl, 10 mM EDTA, 10 mM Na_2HPO_4, 0.5% NP-40, 0.1% SDS, 10 mM NaF, and Ser/Thr- and Tyr-phosphatase inhibitor cocktails. Protein A agarose beads (Santa Cruz Biotechnology) washed in the same buffer were added, and incubation continued for 2 hr. The beads were collected by centrifugation and washed five times with buffer A. Samples were resuspended in sample buffer for SDS-PAGE, and the mixture was boiled for 5 min. Beads were pelleted by centrifugation, and supernatants were applied to 7.5% SDS-PAGE. The following antibodies were used: goat anti-IL1RAPL1 (R&D Systems) at dilution 1:1000, rabbit anti-Homer1 (gift from E. Kim, KAIST) at 1:500, rabbit anti-HA-tag (Santa Cruz Biotechnology), and mouse anti-HA-tag (Roche Applied Science).

Primary Rat Hippocampal Neurons and Cell Cultures, Transfection, Staining, and Quantification

Low-density hippocampal neuronal cultures were prepared from E18–E19 rat hippocampi as previously described with minor modifications [27] and grown in 12-well Petri dishes (Iwaki). Neurons were transfected via calcium phosphate precipitation method at DIV9, and transfected cells were used 7 days after transfection.

African green monkey kidney (COS-7) or HEK293T cells at 50%–70% confluency (24 hr after plating in 6-well plates or on glass coverslips in 12-well plates) were transfected by Lipofectamine 2000 transfection reagent (Invitrogen) with cDNA expression constructs (1–2 μg DNA per well) for 2–3 hr at 5% CO_2, 37°C. Cells were washed twice with phosphate-buffered saline (PBS), fed with Dulbecco's modified Eagle's medium, 10% fetal bovine serum, 1% penicillin/streptomycin, and grown for 24–48 hr before fixation for immunocytochemistry or before lysis for coimmunoprecipitation or pull-down assay.

Hippocampal neurons or COS-7 cells were fixed in 4% paraformaldehyde (PFA)-4% sucrose for 10 min. Primary (1:50–1:100) and secondary (1:200) antibodies were applied in gelatin detergent buffer (30 mM phosphate buffer [pH 7.4] containing 0.2% gelatin, 0.5% Triton X-100, and 0.8 M NaCl).

Confocal images were obtained with an LSM 510 Meta confocal microscope (Carl Zeiss; a gift from F. Monzino) and a 63× objective (numerical aperture 1.4) with sequential acquisition settings of 1024 × 1024 pixels. Each image was a Z series projection of about 7–15 images, each averaged two to four times and taken at 0.4–0.7 μm depth intervals. Morphometric analysis and quantification of synaptic clusters were performed with MetaMorph software (Molecular Devices) by investigators who were blind to type of transfection and experimental manipulation. Colocalization was measured by color-separating PSD-95, Shank, synaptophysin, and vGAT channels, manually setting a threshold level for each channel (identical for each neuron), and then determining the overlapping puncta by manual inspection. PSD-95 and relative pPSD-95 cluster intensity were measured by manually tracing PSD-95 clusters along dendrites of transfected neurons; pPSD-95 intensity was measured only over the PSD-95 clusters in order to eliminate the nonspecific pPSD-95 puncta. Dendritic spine number and dimension were measured as described in [28].

The following commercially available antibodies were used: rabbit anti-IL1RAPL1 antibody (K10) raised with GQRPQTKSSREQNPDEAT peptide (aa 659–677), rabbit anti-HA-tag (Santa Cruz Biotechnology), mouse anti-HA-tag (Roche Applied Science), mouse synaptophysin (Sigma), mouse PSD-95 K28/43 (NeuroMab), guinea pig anti-Shank (gift from E. Kim, KAIST), rabbit anti-VGlut1 (Synaptic System), mouse anti-β-galactosidase (Promega), and rabbit anti-pS-295 PSD-95 (gift from M. Sheng, Massachusetts Institute of Technology).

Preparation of Postsynaptic Density from Mouse Cortex

Subcellular fractions of mouse cortex (five cortices for each genotype) were prepared as described [29]. Briefly, mouse cortex Dounce homogenates (H) were centrifuged at 800 × g to remove nuclei and other large debris. The supernatant was centrifuged at 9,200 × g to obtain a crude synaptosomal fraction (P2), which was subsequently lysed hypo-osmotically and centrifuged at 25,000 × g to pellet a synaptosomal membrane fraction (LP1). LP1 was resuspended and subjected to detergent extraction as described [30] to obtain the PSD-1 and PSD-2 fractions. For all fractions (P2, LP1, PSD-1, and PSD-2), protein concentration was measured via Bradford assay (Bio-Rad) and adjusted before adding Laemmli buffer (Bio-Rad). Thirty micrograms of protein of each fraction was submitted to SDS-PAGE and immunoblotted with a homemade antibody against IL1RAPL1 as described previously [5] or mouse anti-PSD-95 (1:2000; Affinity Bioreagents) antibody. For the western blot experiment of different brain region extracts, we used an antibody against IL1RAPL1 from R&D Systems at dilution 1:1000.

Hippocampal Mouse Neuronal Culture Preparation, Immunostaining, and Quantification

In order to bypass the heterogeneity linked to variation in cell culture conditions, we used a cocultured system between WT and KO neurons where only WT cells express GFP to distinguish them. Embryos used for culture

were generated by crossing an *Il1rapl1*$^{-/-}$ homozygous female with an *Il1rapl1*$^{+/y}$ male with a GFP transgene inserted on its X chromosome. As a result of random X inactivation in females, neurons obtained from pooled embryos expressed either IL1RAPL1 protein together with GFP protein (WT neurons) or no GFP and no IL1RAPL1 (KO neurons). Cultured hippocampal neurons were prepared from embryonic day 18–19 mouse embryos and maintained in Neurobasal B27-supplemented medium (Invitrogen) according to a procedure recommended by Amaxa. At 18 DIV, hippocampal mouse neurons were fixed with 4% PFA in PBS for 5 min at 4°C and for 10 min at room temperature, rinsed three times in PBS followed by a second fixation, and permeabilized with 100% methanol for 6 min at –20°C and one PBS wash (adapted from [31]). Permeabilized cells were blocked for at least 1 hr in PBS 0.2% Tween plus 3% bovine serum albumin and incubated with the appropriate primary and secondary antibodies. The following primary antibodies were used: mouse anti-PSD-95 (1:100; Affinity Bioreagents), rabbit anti-VGlut1 (1:1000, gift from S. El Mestikawy, UPMC), mouse anti-GFP (1:250, Roche Diagnostics), rabbit anti-GFP (1:250, Abcam). Secondary antibodies included fluorescein isothiocyanate donkey anti-mouse or anti-rabbit (1:500; Jackson ImmunoResearch) and Texas red donkey anti-mouse or anti-rabbit (1:1000; Jackson ImmunoResearch). Images were acquired on a Leica DMRA2 microscope. For each genotype, isolated neurons were chosen randomly on the coverslip after checking that no neuron from the other genotype made contact with them. The number of neurons used for quantification is indicated in Figures 3E and 3F. Images were analyzed with ImageJ software (http://rsbweb.nih.gov/ij/). Three independent cocultures were made. For each neuron, mean of cluster intensity and area and the number of cluster per unit of surface were measured. Data were normalized by the mean value of WT from the same culture, and statistical analysis was performed on the pooled data of the three cultures with two-tailed t test (GraphPad Prism 5.1 software).

Electrophysiological Recording on Hippocampal Cultured Neurons

Whole-cell patch-clamp recordings were made from GFP- or IL1RAPL1-transfected rat hippocampal neurons, WT, or IL1RAPL1 KO hippocampal cultured neurons as described above. Patch electrodes, fabricated from thick borosilicate glass, were pulled and fire polished to a final resistance of 3–4 MΩ and filled with the standard internal solution (in mM): 100 CsMES, 20 CsCl, 2 $MgCl_2$, 5 ethylene glycol tetraacetic acid, 10 HEPES, 4 ATP, and 15 phosphocreatine (pH 7.4). EPSCs were investigated in cultured neurons by superfusing the whole-cell clamped neuron with a Tyrode solution containing (in mM): 150 NaCl, 2 $CaCl_2$, 1 $MgCl_2$, 4 KCl, 10 glucose, 10 HEPES (pH 7.4). Neurons were voltage clamped at –70 mV, and TTX (0.3 μM; Tocris) was added to block spontaneous action potential propagation during recording of mEPSCs. All of the experiments were performed at room temperature (22°C–24°C). Statistical analysis was performed with two-tailed t test.

Cortical Mouse Neuronal Culture and Western Blot Experiments

Cultured cortical neurons were prepared from embryonic day 15 mouse embryos and plated at 100,000 cells per 100 mm cell culture dish. At 21 DIV, neurons were treated or not treated for 2.5 hr with 0.1 μM okadaic acid (Calbiochem) or 2 μM TTX (Latoxan). Neurons were then washed with cold PBS and lysed with 500 μl (per plate) of lysis buffer (urea 8 M, 10 mM sodium orthovanadate, 20 mM sodium pyrophosphate, protease inhibitor 1×), and protein concentrations were quantified (Bradford assay, Bio-rad). Samples were diluted in Laemmli buffer with a final concentration 0.5 μg/μl of protein. Cell lysates were submitted to SDS-PAGE and immunoblotted with either mouse anti-pJNK (1:200; Cell Signaling Technology) or rabbit anti-pSer-295 PSD-95 (1:1000; gift from M. Sheng, Genentech) antibody. After stripping (Restore Western Blot Stripping Buffer, Pierce Biotechnology), blots were reprobed with rabbit anti-JNK (1:500; Cell Signaling Technology) or mouse anti-PSD-95 (1:4000; Neuromab), respectively. The number of experiments used for quantification is indicated in Figures 4C–4J. SuperSignal West Femto (Pierce Biotechnology) was used for revelation; acquisition was done with a charge-coupled device (CCD) camera (LAS-3000 Imaging System, Fujifilm), and quantification of band intensity was done with Multi Gauge V3.0. software (Fujifilm). For each lane, level of phosphorylation was determined by dividing band intensity of pJNK or pPSD-95 by total JNK or PSD-95 band intensity. Statistical analysis was performed with two-tailed t test (GraphPad Prism 5.1 software) to compare phosphorylation level of JNK or PSD-95 in KO versus WT cultured neurons in each condition.

Electron Microscopy

IL1RAPL1 KO and WT littermates (at least 3 animals per group) were anaesthetized with an intraperitoneal injection of ketamine-xylazine 1:1 (0.1 ml/kg) and transcardially perfused with ice-cold 2% PFA and 2.5% glutaraldehyde in 0.1 M phosphate buffer (PB; pH 7.4). After perfusion, brains were postfixed in the same solution overnight at 4°C and then washed several times in 0.1 M PB. Vibratome sections (500 μm) were cut through the hippocampus, postfixed with 0.5% osmium tetroxide (in 0.1 M cacodylate buffer) for 20 min on ice, dehydrated in a crescent series of ethanol (30%–100%), and embedded flat with epon-araldite resin in rubber molds. Ultrathin serial sections (70 nm) were cut with an ultramicrotome (Leica Ultracut) and collected on single-slot grids coated with a Pioloform solution. Grids were counterstained with uranyl acetate and lead citrate and were observed in a JEM-1010 electron microscope (JEOL) equipped with a side-mounted CCD camera (Mega View III; Soft Imaging System GmbH). The density of excitatory synapses was evaluated via a stereological method (dissector) on 20 pairs of micrographs of consecutive ultrathin sections for each animal that were taken at 20,000× magnification. To identify a structure as an asymmetric synapse, we followed these criteria: the presence of at least three vesicles within the profile adjacent to the presynaptic membrane and the presence of a clear PSD. Only synapses that were present in the reference section and not in the lookup section were counted. Dendritic spine, presynaptic bouton cross-section area, and PSD length were analyzed on the same images. Dendritic spine heads were recognized by the absence of mitochondria and microtubules and by the presence of a prominent postsynaptic density. To analyze the density of docked and total synaptic vesicles, we photographed 50 randomly chosen synapses per animal at a magnification of 75,000×. Statistical evaluations were performed according to paired Student's t test with Origin 7.0 software.

DiOlistic Labeling of Brain Structures

Fluorescence labeling of neuronal structures was performed as described [32]. Tefzel tubing (Bio-Rad) was placed on a tubing preparation station (Bio-Rad) and filled with polyvinylpyrrolidone (0.32 mg/ml). 1,1′-dioctadecyl-3,3,3′,3′-tetramethylindocarbocyanine perchlorate crystals (DiI; Invitrogen) were dissolved in methylene chloride (Supelco) and then gently dropped onto the tungsten particles (1.3 μm in diameter; Bio-Rad). DiI-coated particles were immersed in distilled water, and the solution was vortexed, sonicated, and then immediately injected into the predried tubing. Finally, the particle-coated tube was rotated and air dried under constant nitrogen flow (0.2 l/min) for 1 hr and subsequently cut into small pieces (microcarriers) that were stored in a desiccated environment at room temperature. IL1RAPL1 KO mice and WT littermates (at least 4 animals per group) were anesthetized with an intraperitoneal injection of ketamine-xylazine 1:1 (0.1 ml/kg) and perfused with PBS, and then with 4% PFA in 0.1 M PB. Brains were postfixed in the same fixative solution, washed several times in PB 0.1 M, and then cut into 300 μm sections on a vibratome (Leica VT 1000S). A commercially available helios gene gun system (Bio-Rad) was used to propel DiI-coated particles into fixed slices. A membrane filter with a 3.0 μm pore size (Millipore) was placed between the gun and the tissue to filter out large clusters of coated particles. The particles were accelerated with inert helium gas (120 pounds per square inch [psi]). After the shot, the slices were placed in 4% PFA for 2 hr, washed 3 times in PB 0.1 M, and mounted on glass slides. A confocal microscope (Zeiss LSM-5 Pascal) equipped with a 40× oil-immersion objective was used to acquire images from fluorescently labeled secondary and tertiary branches of apical and basal dendrites in the stratum radiatum of CA1 area in the hippocampus. At least 10 Z stack images consisting of 10–15 sections (512 × 512 pixels, 80 to 100 μm-long dendritic segments) spaced 0.5 μm apart were collected for each animal and for each area analyzed to generate the data set. Dendritic segments and spines were analyzed quantitatively with ImageJ software 1.34S (NIH, public domain), with the observer blinded to the experimental conditions. All dendritic protrusions with a clearly recognizable neck connected to the shaft of the dendrite were counted as spines. Measure of spine density was performed on projected Z stack. If dendritic spines were too packed to clearly separate them from each other, we turned to serial stack images to delineate individual spines. By scrolling through the stack of different optical sections, we could identify individual spine heads with larger confidence. For presentation, digital micrographs were processed with the software IMARIS. Files were imported into Adobe Photoshop, where images were cropped. Statistical analysis was performed by paired Student's t test.

Hippocampal Slice Preparation and Electrophysiology

KO and WT mice were sacrificed by cervical dislocation. Brains were removed from the skull, and the hippocampi were quickly dissected out in ice-cold oxygenated artificial cerebrospinal fluid (ACSF) containing the

following (in mM): 120 NaCl, 2.5 KCl, 2.5 $CaCl_2$, 1.2 $MgCl_2$, 26.2 $NaHCO_3$, 1.0 NaH_2PO_4, 11.0 glucose, bubbled with a mixture of 95% O2/5% CO_2 (pH 7.4). Transverse hippocampal slices (400 μM) were cut with a manual tissue chopper (Stoelting) and maintained in a humidified holding chamber at room temperature for at least 1 hr for recovery [33]. Slices were then individually transferred to an interface recording chamber (Fine Science Tools) where they were continuously perfused with ACSF maintained at 29°C and at a flowing rate of 1.5–2 ml/min. Extracellular field excitatory postsynaptic potentials (fEPSPs) were recorded in stratum radiatum of area CA1 of the hippocampus with glass electrodes filled with 1 M NaCl coupled to the input stage of a Warner IE-210 amplifier. Stimuli were delivered (0.1 ms pulse duration) to the commissural/Schaffer collateral afferents at a frequency of 0.033 Hz (for long-term potentiation [LTP] and long-term depression [LTD] experiments) or 0.1 Hz (for input-output and PPF experiments) with a concentric bipolar stainless steel electrode. For LTD experiments, a stimulus intensity that elicited a fEPSP amplitude that was ~50% of maximum was used. For LTP experiments, starting fEPSP amplitude was ~33% of maximum. Synaptic efficacy curve was built by measuring the fiber volley and fEPSP of the responses evoked by stimulating afferent fibers with current intensities ranging from 20 to 300 μA. PPF was induced by applying pairs of stimuli at the following interstimulus intervals (in ms): 10, 25, 50, 75, 100, 150, 200, 250, and 300. LTP was induced either by high-frequency stimulation (3 trains of 100 stimuli at 100 Hz, with 10 s intertrain interval) or by TBS (16 bursts of 5 stimuli at 100 Hz, with 200 ms interburst intervals). For LTD, a low-frequency stimulation (900 stimuli at 1 Hz) was used. The presynaptic fiber volley was measured as the amplitude to the negative peak that appears after the stimulus artifact. Synaptic activity was measured as the maximal slope of the rising phase of the fEPSP. Data are presented as means ± standard error of the mean. Statistical analysis was performed by one-way ANOVA.

Supplemental Information

Supplemental Information includes Supplemental Experimental Procedures and six figures and can be found with this article online at doi:10.1016/j.cub.2009.12.030.

Acknowledgments

We thank M. Sheng for the anti pSer-295-PSD-95 and M. Okabe for the XGFP transgenic mice. J.B. was supported by the Czech Science Foundation (grant GACR303/08/1591), the Academy of Sciences of the Czech Republic (institutional project AV0Z50520514), and the Ministry of Education, Youth and Sports of the Czech Republic (VZ MSM 0021620820). M.G. was supported by Telethon Italy (grant GGP05236A) and Compagnia di San Paolo. H.V. was supported by a fellowship from the Spanish Ministerio de Educación y Ciencia (EX2006-0294). P.B. was supported by Agence Nationale pour la Recherche (projects ANR-05-Neuro-040-01 and ANR-06-Neuro-003-02), Fondation Jerome Lejeune, and Inserm. C.S. was supported by grants from Telethon Italy (grant GGP06208), Fondazione Cariplo (project 2006-0779), Compagnia di San Paolo (project 2005.1964), RSTL-CNR, and PRIN 2007. M.P. was supported by Fondazione Cariplo (project 2008-2318).

Received: July 21, 2009
Revised: November 25, 2009
Accepted: December 4, 2009
Published online: January 21, 2010

References

1. Chelly, J., Khelfaoui, M., Francis, F., Chérif, B., and Bienvenu, T. (2006). Genetics and pathophysiology of mental retardation. Eur. J. Hum. Genet. *14*, 701–713.
2. Carrié, A., Jun, L., Bienvenu, T., Vinet, M.C., McDonell, N., Couvert, P., Zemni, R., Cardona, A., Van Buggenhout, G., Frints, S., et al. (1999). A new member of the IL-1 receptor family highly expressed in hippocampus and involved in X-linked mental retardation. Nat. Genet. *23*, 25–31.
3. Laumonnier, F., Shoubridge, C., Antar, C., Nguyen, L.S., Van Esch, H., Kleefstra, T., Briault, S., Fryns, J.P., Hamel, B., Chelly, J., et al. (2009). Mutations of the UPF3B gene, which encodes a protein widely expressed in neurons, are associated with nonspecific mental retardation with or without autism. Mol. Psychiatry. Published online February 24, 2009. 10.1038/mp.2009.14.
4. Piton, A., Michaud, J.L., Peng, H., Aradhya, S., Gauthier, J., Mottron, L., Champagne, N., Lafrenière, R.G., Hamdan, F.F., Joober, R., et al. S2D team (2008). Mutations in the calcium-related gene IL1RAPL1 are associated with autism. Hum. Mol. Genet. *17*, 3965–3974.
5. Bahi, N., Friocourt, G., Carrié, A., Graham, M.E., Weiss, J.L., Chafey, P., Fauchereau, F., Burgoyne, R.D., and Chelly, J. (2003). IL1 receptor accessory protein like, a protein involved in X-linked mental retardation, interacts with Neuronal Calcium Sensor-1 and regulates exocytosis. Hum. Mol. Genet. *12*, 1415–1425.
6. Gambino, F., Pavlowsky, A., Béglé, A., Dupont, J.L., Bahi, N., Courjaret, R., Gardette, R., Hadjkacem, H., Skala, H., Poulain, B., et al. (2007). IL1-receptor accessory protein-like 1 (IL1RAPL1), a protein involved in cognitive functions, regulates N-type Ca2+-channel and neurite elongation. Proc. Natl. Acad. Sci. USA *104*, 9063–9068.
7. Ehrlich, I., Klein, M., Rumpel, S., and Malinow, R. (2007). PSD-95 is required for activity-driven synapse stabilization. Proc. Natl. Acad. Sci. USA *104*, 4176–4181.
8. El-Husseini, A.E., Schnell, E., Chetkovich, D.M., Nicoll, R.A., and Bredt, D.S. (2000). PSD-95 involvement in maturation of excitatory synapses. Science *290*, 1364–1368.
9. Born, T.L., Smith, D.E., Garka, K.E., Renshaw, B.R., Bertles, J.S., and Sims, J.E. (2000). Identification and characterization of two members of a novel class of the interleukin-1 receptor (IL-1R) family. Delineation of a new class of IL-1R-related proteins based on signaling. J. Biol. Chem. *275*, 41528.
10. Khan, J.A., Brint, E.K., O'Neill, L.A., and Tong, L. (2004). Crystal structure of the Toll/interleukin-1 receptor domain of human IL-1RAPL. J. Biol. Chem. *279*, 31664–31670.
11. Kim, M.J., Futai, K., Jo, J., Hayashi, Y., Cho, K., and Sheng, M. (2007). Synaptic accumulation of PSD-95 and synaptic function regulated by phosphorylation of serine-295 of PSD-95. Neuron *56*, 488–502.
12. Gambino, F., Kneib, M., Pavlowsky, A., Skala, H., Heitz, S., Vitale, N., Poulain, B., Khelfaoui, M., Chelly, J., Billuart, P., and Humeau, Y. (2009). IL1RAPL1 controls inhibitory networks during cerebellar development in mice. Eur. J. Neurosci. *30*, 1476–1486.
13. Sheng, M., and Sala, C. (2001). PDZ domains and the organization of supramolecular complexes. Annu. Rev. Neurosci. *24*, 1–29.
14. Yoon, S., Choi, J., Yoon, J., Huh, J.W., and Kim, D. (2006). Okadaic acid induces JNK activation, bim overexpression and mitochondrial dysfunction in cultured rat cortical neurons. Neurosci. Lett. *394*, 190–195.
15. Otto, C., Kovalchuk, Y., Wolfer, D.P., Gass, P., Martin, M., Zuschratter, W., Gröne, H.J., Kellendonk, C., Tronche, F., Maldonado, R., et al. (2001). Impairment of mossy fiber long-term potentiation and associative learning in pituitary adenylate cyclase activating polypeptide type I receptor-deficient mice. J. Neurosci. *21*, 5520–5527.
16. Farías, G.G., Alfaro, I.E., Cerpa, W., Grabowski, C.P., Godoy, J.A., Bonansco, C., and Inestrosa, N.C. (2009). Wnt-5a/JNK signaling promotes the clustering of PSD-95 in hippocampal neurons. J. Biol. Chem. *284*, 15857–15866.
17. Björkblom, B., Ostman, N., Hongisto, V., Komarovski, V., Filén, J.J., Nyman, T.A., Kallunki, T., Courtney, M.J., and Coffey, E.T. (2005). Constitutively active cytoplasmic c-Jun N-terminal kinase 1 is a dominant regulator of dendritic architecture: Role of microtubule-associated protein 2 as an effector. J. Neurosci. *25*, 6350–6361.
18. Gdalyahu, A., Ghosh, I., Levy, T., Sapir, T., Sapoznik, S., Fishler, Y., Azoulai, D., and Reiner, O. (2004). DCX, a new mediator of the JNK pathway. EMBO J. *23*, 823–832.
19. Lein, E.S., Hawrylycz, M.J., Ao, N., Ayres, M., Bensinger, A., Bernard, A., Boe, A.F., Boguski, M.S., Brockway, K.S., Byrnes, E.J., et al. (2007). Genome-wide atlas of gene expression in the adult mouse brain. Nature *445*, 168–176.
20. Albensi, B.C., Oliver, D.R., Toupin, J., and Odero, G. (2007). Electrical stimulation protocols for hippocampal synaptic plasticity and neuronal hyper-excitability: Are they effective or relevant? Exp. Neurol. *204*, 1–13.
21. Boda, B., Mas, C., and Muller, D. (2002). Activity-dependent regulation of genes implicated in X-linked non-specific mental retardation. Neuroscience *114*, 13–17.
22. Raymond, C.R., and Redman, S.J. (2006). Spatial segregation of neuronal calcium signals encodes different forms of LTP in rat hippocampus. J. Physiol. *570*, 97–111.
23. Paterlini, M., Revilla, V., Grant, A.L., and Wisden, W. (2000). Expression of the neuronal calcium sensor protein family in the rat brain. Neuroscience *99*, 205–216.

24. Vacher, H., Mohapatra, D.P., and Trimmer, J.S. (2008). Localization and targeting of voltage-dependent ion channels in mammalian central neurons. Physiol. Rev. *88*, 1407–1447.
25. Migaud, M., Charlesworth, P., Dempster, M., Webster, L.C., Watabe, A.M., Makhinson, M., He, Y., Ramsay, M.F., Morris, R.G., Morrison, J.H., et al. (1998). Enhanced long-term potentiation and impaired learning in mice with mutant postsynaptic density-95 protein. Nature *396*, 433–439.
26. Takagi, N., Sugimoto, M., Yamaguchi, S., Ito, M., Tan, S.S., and Okabe, M. (2002). Nonrandom X chromosome inactivation in mouse embryos carrying Searle's T(X;16)16H translocation visualized using X-linked LACZ and GFP transgenes. Cytogenet. Genome Res. *99*, 52–58.
27. Sala, C., Piëch, V., Wilson, N.R., Passafaro, M., Liu, G., and Sheng, M. (2001). Regulation of dendritic spine morphology and synaptic function by Shank and Homer. Neuron *31*, 115–130.
28. Piccoli, G., Verpelli, C., Tonna, N., Romorini, S., Alessio, M., Nairn, A.C., Bachi, A., and Sala, C. (2007). Proteomic analysis of activity-dependent synaptic plasticity in hippocampal neurons. J. Proteome Res. *6*, 3203–3215.
29. Huttner, W.B., Schiebler, W., Greengard, P., and De Camilli, P. (1983). Synapsin I (protein I), a nerve terminal-specific phosphoprotein. III. Its association with synaptic vesicles studied in a highly purified synaptic vesicle preparation. J. Cell Biol. *96*, 1374–1388.
30. Cho, K.O., Hunt, C.A., and Kennedy, M.B. (1992). The rat brain postsynaptic density fraction contains a homolog of the Drosophila discs-large tumor suppressor protein. Neuron *9*, 929–942.
31. Brock, R., Hamelers, I.H., and Jovin, T.M. (1999). Comparison of fixation protocols for adherent cultured cells applied to a GFP fusion protein of the epidermal growth factor receptor. Cytometry *35*, 353–362.
32. Gan, W.B., Grutzendler, J., Wong, W.T., Wong, R.O., and Lichtman, J.W. (2000). Multicolor "DiOlistic" labeling of the nervous system using lipophilic dye combinations. Neuron *27*, 219–225.
33. Vara, H., Onofri, F., Benfenati, F., Sassoè-Pognetto, M., and Giustetto, M. (2009). ERK activation in axonal varicosities modulates presynaptic plasticity in the CA3 region of the hippocampus through synapsin I. Proc. Natl. Acad. Sci. USA *106*, 9872–9877.